Two-dimensional solutions and analytical–numerical intercomparison

Supplementary document for
"Marine ice sheet dynamics: the impacts of ice-shelf buttressing"

by Sam Pegler

This supplementary document presents the results of full two-dimensional numerical simulations and compares them to the predictions of the quasi-one-dimensional (Q1D) model defined by (2.9) and (2.11) in the paper. The aim is to provide a demonstration of the accuracy of the Q1D model for general planform aspect ratios (spanning the full range of wide to narrow channel geometries), thereby testing the robustness of the heuristic lateral drag approximation (2.11).

1 Two-dimensional equations

Consider a marine ice sheet flowing in a parallel-walled channel of uniform width $2w$. The two-dimensional thin film equations describing the flow are

$$\boldsymbol{\nabla}\cdot[\mu H(\mathbf{e}+(\boldsymbol{\nabla}\cdot\boldsymbol{u})\mathbf{I})]-\tau_b(\boldsymbol{u})\hat{\boldsymbol{u}}=\rho gH\boldsymbol{\nabla}h, \tag{1}$$

$$\frac{\partial H}{\partial t}+\boldsymbol{\nabla}\cdot(H\boldsymbol{u})=f(x,t), \tag{2}$$

where $\tau_b=\mu_0|\boldsymbol{u}/\lambda_-|^m$ (e.g. MacAyeal, 1989). The no-slip condition on the sidewalls is

$$\boldsymbol{u}=\mathbf{0}\qquad\text{on } y=w, \tag{3}$$

I impose an ice divide at $x=x_D$ at which the symmetry condition

$$\boldsymbol{u}=\mathbf{0}\qquad\text{on } x=x_D \tag{4}$$

applies. Along a calving front at $x=x_C$, I impose the stress condition

$$\hat{\boldsymbol{n}}\cdot\mathbf{e}+(\boldsymbol{\nabla}\cdot\boldsymbol{u})\hat{\boldsymbol{n}}=(\rho gH/4)\hat{\boldsymbol{n}}\qquad\text{on } x=x_C, \tag{5}$$

where $\hat{\boldsymbol{n}}=\hat{\boldsymbol{x}}$ is the unit outward horizontal normal to the calving front. I imposed a distributed input over an interval of length $l\equiv x_\infty-x_D$ downstream of the ice divide,

$$f(x,t)=\begin{cases} f_0 & x_D\le x\le x_\infty,\\ 0 & \text{elsewhere.}\end{cases} \tag{6}$$

This conditions produces a steady-state input flux of $Q = 2wlf_0$ for $x > x_\infty$. This corresponds to the same input condition downstream of x_∞ as assumed in the numerical examples of the paper.

1.1 Dimensionless equations

Non-dimensionalisation using the intrinsic thickness and length scales, $\mathcal{H}$ and $\mathcal{L}$, defined by $(2.20a, b)$ in the paper yields the following dimensionless system of equations

$$\boldsymbol{\nabla} \cdot [\mu H(\mathbf{e} + (\boldsymbol{\nabla} \cdot \boldsymbol{u})\mathbf{I})] - \tau_b(\boldsymbol{u})\hat{\boldsymbol{u}} = H\boldsymbol{\nabla} h, \tag{7}$$

$$\frac{\partial H}{\partial t} + \boldsymbol{\nabla} \cdot (H\boldsymbol{u}) = F(x,t), \tag{8}$$

where $\tau_b = |\boldsymbol{u}|^m$. The no-slip conditions at the ice divide and the lateral margins are

$$\boldsymbol{u} = \mathbf{0} \qquad \text{on } x = X_D, \tag{9}$$

$$\boldsymbol{u} = \mathbf{0} \qquad \text{on } y = W \equiv (C/S)^{n/(n+1)}, \tag{10}$$

where $X_D \equiv x_D/\mathcal{L}$ and $W \equiv w/\mathcal{L}$, and $C \equiv 2[1 + (n/2)]^{1/n}$ is a constant equal to $C \approx 2.115$ for $n = 3$. The dynamic boundary condition (5) is

$$\hat{\boldsymbol{n}} \cdot \mathbf{e} + (\boldsymbol{\nabla} \cdot \boldsymbol{u})\hat{\boldsymbol{n}} = (\delta H/4)\hat{\boldsymbol{n}} \qquad \text{on } x = X_C, \tag{11}$$

where $X_C \equiv x_C/\mathcal{L}$. The accumulation condition (6) is

$$F(x,t) = \begin{cases} 1/(2LW) & x_{div} \le x \le x_\infty, \\ 0 & \text{elsewhere,} \end{cases} \tag{12}$$

where $L \equiv l/\mathcal{L}$. The dimensionless steady-state flux per unit width arising for $x > X_\infty$ is

$$\frac{1}{2W}\int_{-W}^{W} Hu \, \mathrm{d}y = 1. \tag{13}$$

Equations (7)–(12) comprise a coupled hyperbolic–elliptic problem for the two-dimensional evolution of the thickness $H(x, y, t)$. I solve these equations using the adaptive finite-element solver Úa developed by G. Hilmar Gudmundsson (Gudmundsson *et al.*, 2012; Gudmundsson, 2013). The solver was initialised using the steady-state solution to the Q1D model, described by (3.1)–(3.2) in the paper, and allowed to relax towards a steady state. For these examples, I consider the power-law case $n = 3$, set the dimensionless calving position as $x_C = 6000$, and assume the negatively-sloped bed profile

$$b = -\beta + \alpha x \tag{14}$$

where $\alpha = -10^{-3}$ and $\beta = 6$.

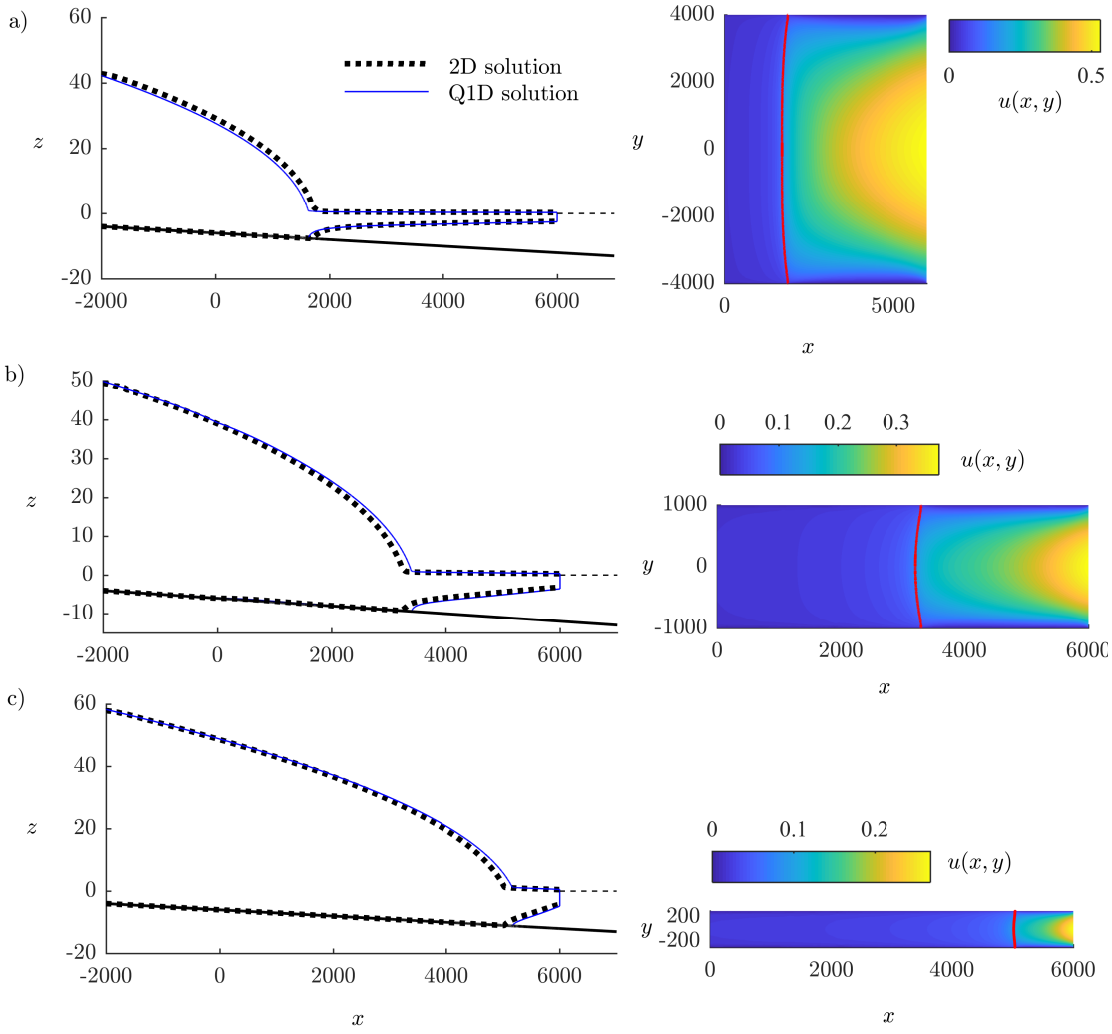

Figure 1: Numerical predictions for the dimensionless width-averaged thickness profile in steady state, $\bar{H}(x)$ (left), and two-dimensional longitudinal velocity field, $u(x, y)$, for dimensionless channel half widths (a) $W = 4000$, (b) 1000 and (c) 300 obtained from numerical solutions of the full two-dimensional equations . The left-hand plots show the width-averaged surface profiles: the dotted black curves shows the numerical solutions of the full two-dimensional model ('2D solution') obtained using finite-element analysis; the continuous blue curves show the prediction of the quasi-one-dimensional theory ('Q1D solution') given by the solution of (3.1)–(3.2) of the paper. The right-hand plots show the planform two-dimensional longitudinal velocity field $u(x, y)$ obtained from the two-dimensional solution. The red curve shows the grounding line in each case.

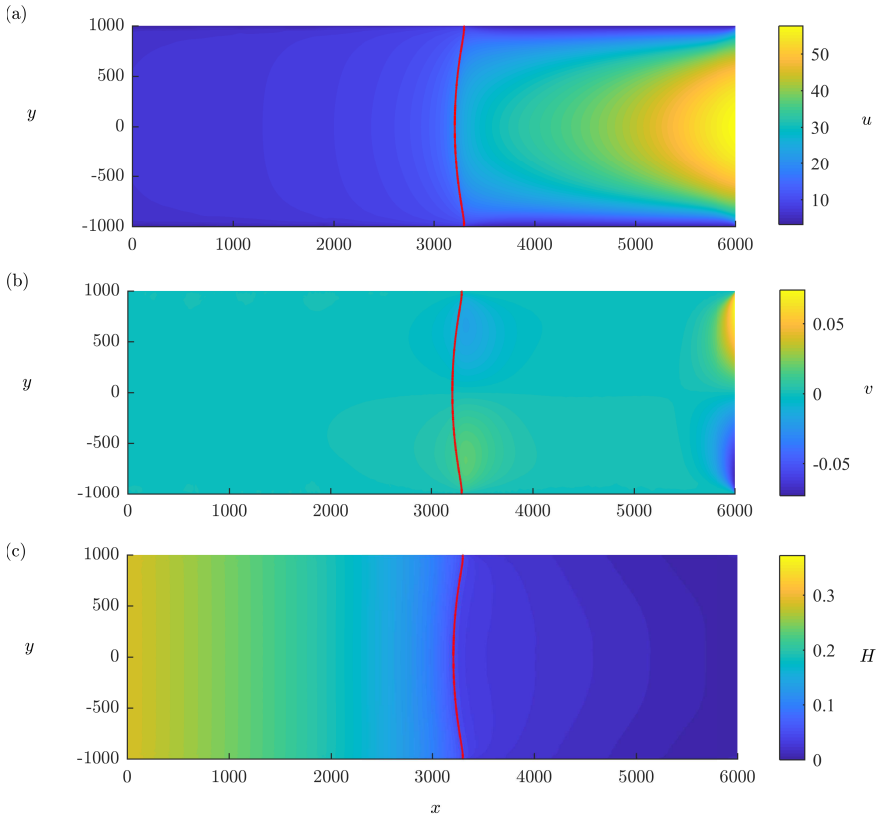

Figure 2: Numerical solutions for (a) the longitudinal velocity $u(x, y)$, (b) the transverse velocity $v(x, y)$, and (c) the thickness $H(x, y)$, in steady state for dimensionless channel half width $W = 1000$ obtained from finite-element integration of the full two-dimensional equations (7)–(12). The grounding line is shown as a red curve in each panel.

2 Results

The steady states thus determined for three dimensionless channel half widths: (a) $W = 4000$ (b) 1000 and (c) 300 are shown in figure 1. The corresponding longitudinal velocity field $u(x, y)$ is shown by the colour plots on the right-hand side. The left-hand plots show the width-averaged profile of the marine ice sheet, i.e. the surface height

$$\bar{h}(x) = \frac{1}{2W} \int_{-W}^{W} h(x, y) \, \mathrm{d}y. \tag{15}$$

For each case, the prediction of the two-dimensional equations (7)–(12) is shown by the dotted black curves. The corresponding prediction of the Q1D given by solving (3.1)–(3.2) of the paper are shown by solid blue curves. The right-hand panels show the longitudinal velocity field $u(x, y)$ given by the 2D solution, with the grounding line shown by the red curve. There is generally excellent agreement across the complete range of planform aspect ratios. The best absolute agreement occurs for the largest channel width [case (a)], for which the ice shelf is wider than it is long. Very good agreement similarly applies to the intermediate case (b), for which the ice shelf produced is 1.2 times longer than it is wide, and in the narrowest case (c), for which the ice shelf produced is 4 times longer than it is wide. Despite some considerable cross-channel two-dimensional deformation shown the right-hand panels, the Q1D theory describes the two-dimensional marine ice sheets accurately across the fully range of planform aspect ratios.

Figure 2 shows the planform longitudinal velocity field $u(x, y)$, transverse velocity $v(x, y)$ and thickness field $H(x, y)$ for the intermediate example (b). The transverse velocity $v(x, y)$ becomes relatively larger in the immediate front of the grounding line, representing a feature of the so-called 'inlet boundary layer' discussed in §5.1 of the paper. There is also a considerable increase in lateral velocity at the corners of the calving front, which can be interpreted as a corner flow that feeds a hypothetical die swell downstream of the channel mouth (Pegler, 2016). Another interesting feature illustrated by the thickness field $H(x, y)$ near the grounding line is that the ice sheet is thicker towards the margin. This feature is also indicated by the direction of curvature of the grounding line. Further downstream, however, the flow transitions to becoming thickest instead along its centreline, with a transition from the grounding line involving three localised maxima in thickness across the transverse section. Despite these complex two-dimensional features, the Q1D model satisfactory describes the large-scale dynamics.

References

Gudmundsson, G. H. 2013 Ice-shelf buttressing and the stability of marine ice sheets. *The Cryosphere* **7**, 647–655.

Gudmundsson, G. H., Krug, J., Durand, G., Favier, L. & Gagliardini, O. 2012 The stability of grounding lines on retrograde slopes. *The Cryosphere* **6**, 1497–1505.

MacAyeal, D. R. 1989 Large-scale ice flow over a viscous basal sediment: Theory and application to Ice Stream B, Antarctica. *J. Geophys. Res.* **94**, 4071–4087.

Pegler, S. S. 2016 The dynamics of confined extensional flows. *J. Fluid Mech.* **804**, 24–57.